LEVEL II

(12)

LASER ASSISTED HOT SPOT MACHINING

(12) (19)

ARPA Order No. 3421

Program Code No. NR 039-I45

Contractor: University of Southern California

Contract Date: June 1, 1977

Contract Amount: $170,162.00

(15) Contract No. N00014-77-C-0478 and ARPA Order-3421

Contract Expiration Date: May 31, 1979

(6) Title: Laser Assisted Hot Spot Machining.

Principal Investigators: (10) S. M. Copley, M. Bass, E. Garmire

(213) 741-6418

(9) Status rept no. 7, Dec 78-Feb 79

R & D Status Report Number 7

(11) Feb 79

During the quarter (December 1978 - February 1979) the major activity in this program was the development of scaling rules for laser aided machining and for laser machining of ceramics. These are discussed in detail in the attached copy of the paper we will present at the ASM Conference on Laser Materials Interactions in Washington, DC in April. Some additional results are presented below:

Figure 1 shows the relationship of the laser beam cutting tool and work piece. In an experiment on Inconel 718 without laser heating, we measured a cutting force F_x = 206 N and a friction force F_y = 132 N under the following conditions: cutting velocity, V = 15.2 cm Sec^{-1}; feed, f = 0.025 mm;

JCB

depth of cut, a_c = 0.50 mm; and rake angle $\delta_{ne} = 0^o$. By taking the ratio (r_c) of the measured chip thickness, a_c = 0.127 mm, to the feed, we calculated a shear plane angle $\phi = 11.1^o$.

Fig. 2 shows the temperature (T) and yield stress (σ) of Inconel 718 as a function of distance, ζ, along the shear plane. Curves T_0 and σ_0 correspond to no laser heating. From F_x and V, the machining power (P_m) can be calculated and is 31.2 J S^{-1}. From F_y, V and r_c, the power dissipated due to shearing at the rake face of the tool (P_f) can be calculated and is 7.8 J S^{-1}, The difference, $P_m - P_f$, gives the heat liberated on the shear plane associated with the formation of the chip. The analysis of Weiner (Trans ASME 77, 1331 (1955)) was employed to calculate T_o from the heat liberated. The corresponding values of yield stress were obtained from the International Nickel Data Book, Curves T_{450} and σ_{450}, and T_{1400} and σ_{1400} correspond to heating with a 450 W and a 1400 W laser beam focused to a beam diameter of 130 μm, respectively. The laser beam was incident on the workpiece 0.4 cm in front of the edge of the cutting tool. The temperature due to laser heating was calculated based on the analysis of Cline and Anthony (J. Appl. Phys. 48, 3895 (1977)). The approximate location of the solidus isotherms in the vicinity of the laser beam for both incident powers are shown in the sketch.

The temperatures, T_{450} and T_{1400}, are calculated by superimposing the effects of laser heating and shear plane heating.

Figs. 1 and 2 show that at both 450 W and 1400 W the tool cuts through melted and rapidly quenched material. This treatment should dissolve large carbides present in the material and reprecipitate them in a fine dispersion which may lead to a reduction in a tool wear. Also, it will radically change the morphology of the hardening precipitates, which may improve machinability by decreasing the tendency to form a built up edge. Figs. 1 and 2 also show that the laser causes a significant change in temperature at the shear plane. At 450 W, laser heating results in a dramatic reduction in yield stress along the shear plane. At 1400 W, it appears that the combined effects of beam and shear plane heating produce melting across two thirds of the chip.

Other activities included receipt, installation and testing of the Kistler 3 axis tool for a measurement system. With this major diagnostic device operating, we will renew our LAM experiments in the next quarter. The infrared imaging pyroelectric vidicon TV system purchased through and NSF equipment grant has been received and tested. This system will be used to measure laser beam distributions and laser induced heating.

Experiments on laser shaping hot pressed Si_3N_4 have been resumed using the 1400 W CO_2 laser at 1000 W. Initial

tests performed with a 63 mm focal length lens, an N_2 gas flow along the laser beam, and a surface speeds of 0.42 cm/sec showed material removal depths of 0.5 cm. Tests with an O_2 gas jet show deeper grooves and suggest that the material removal process is a form of laser induced burning at temperatures which result in volatile combustion products. This idea will be pursued further and may help in rough shaping ceramics. A lapidary diamond saw was purchased to expedite cutting samples and sectioning laser grooved material for microscopy.

LAM OF INCONEL 718

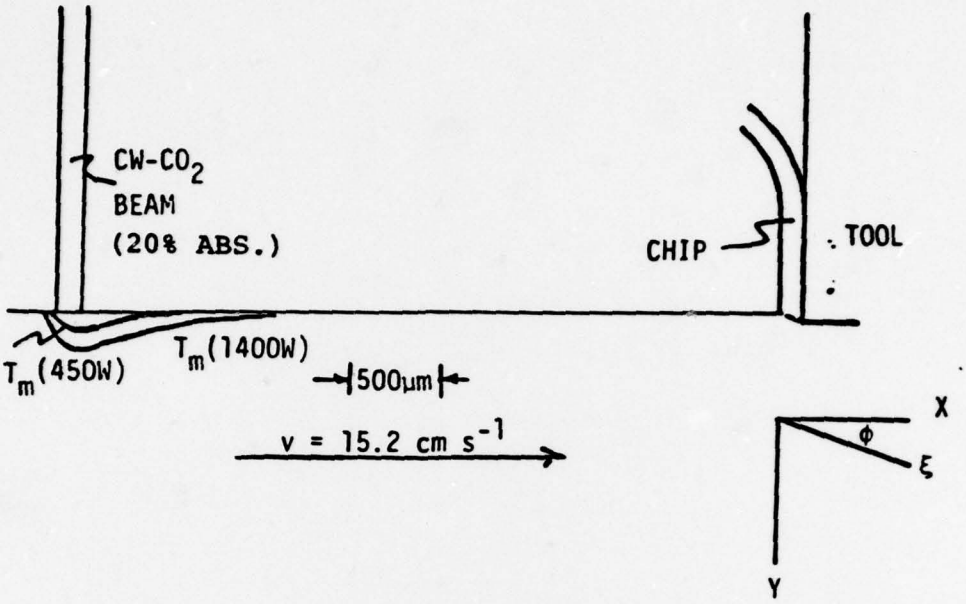

Figure 1

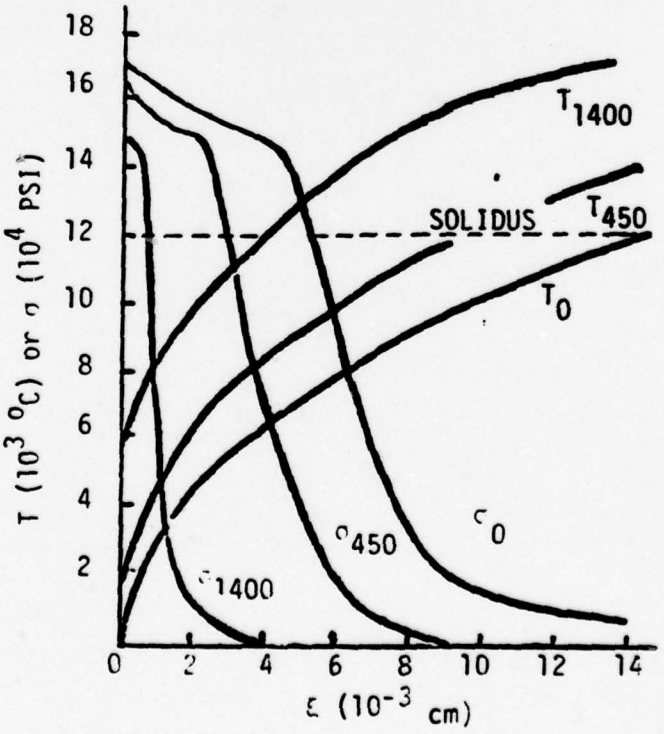

Figure 2

SHAPING MATERIALS WITH A CONTINUOUS WAVE CARBON DIOXIDE LASER

Stephen M. Copley
Michael Bass
University of Southern California
Los Angeles, California

Although the use of carbon dioxide lasers for straight line cutting and hole drilling is well established (1), their application to turning is recent (2,3). In our work, the laser beam is initially directed along a path that is parallel to the turning axis of a lathe, Fig. 1. It is then reflected from a mirror mounted on the carriage along a direction perpendicular to the turning axis to a mirror mounted on the cross-slide. After reflection from the cross-slide mirror, it is focussed by a ZnSe lens on the workpiece. Because the direction of motion of the carriage is parallel to the turning axis and the direction of motion of the cross-slide is perpendicular to the turning axis, the angular relationships of the reflected beams remain constant during turning and facing operations.

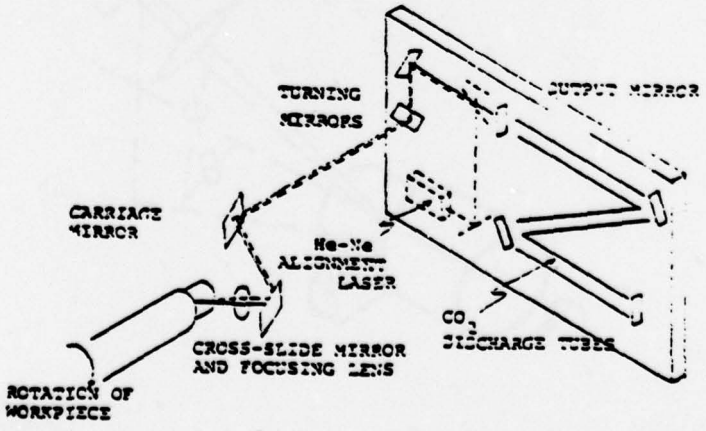

Fig. 1. Arrangement for laser assisted machining and laser machining.

We have employed two approaches to shape materials by turning with a laser: laser assisted machining, where the laser heats a volume of material directly in front of the single point cutting tool; and laser machining, where the laser vaporizes the material. Figure 2 shows the arrangement for laser assisted machining, which has been used primarily in shaping metals and alloys. In our initial experiments $\theta = 30^{\circ}$ and $\phi = 20^{\circ}$. In order to avoid interference by the chip, the beam was focussed on the workpiece 0.4cm ahead of the cutting tool. In laser machining, which has been used primarily in shaping silicon compound ceramics, $\theta = 90^{\circ}$, the beam direction intersects the turning axis and no cutting tool is employed.

LASER ASSISTED MACHINING

Figure 3 shows a top view of the workpiece, cutting tool and laser beam with the chip removed. By setting the major cutting edge angle (κ_r) equal to $\pi/2 - \theta$, it is possible to minimize the area of the beam falling on the workpiece and thus maximize the incident power density. The back engagement (depth of cut) is a_p and should approximately equal the beam diameter. The distance moved by the tool parallel to the turning axis per revolution (feed) is f.

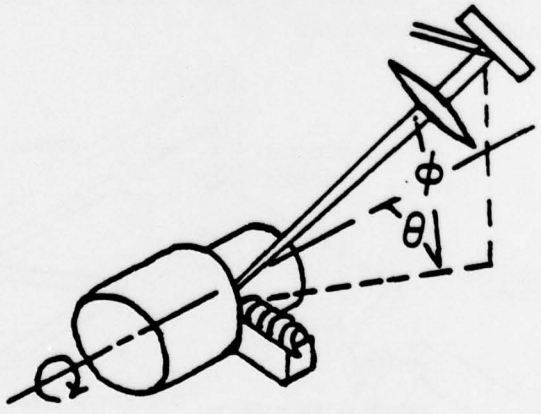

Fig. 2. Relationship of beam and workpiece for laser assisted machining.

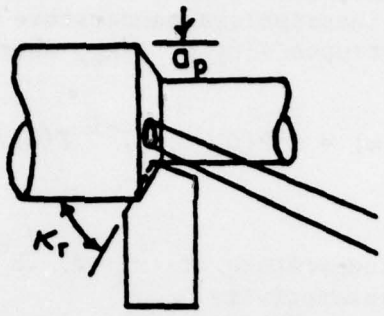

Fig. 3. Top view of workpiece laser beam and cutting tool with chip omitted.

Temperature Distribution

Figure 4 shows a view of the workpiece, cutting tool and laser beam looking parallel to the turning axis. The temperature distribution will be described in a coordinate system such that the z axis is parallel to the laser beam and the y axis is tangent to the workpiece surface at the beam impingement point. For simplicity, it is assumed that the laser beam is perpendicular to the workpiece surface. To calculate the depth of the melted region $s(T_m)$ or austenitized region $s(T_c)$, we employ the thermal analysis of Cline and Anthony for a Gaussian heat source moving at a constant velocity. (4)

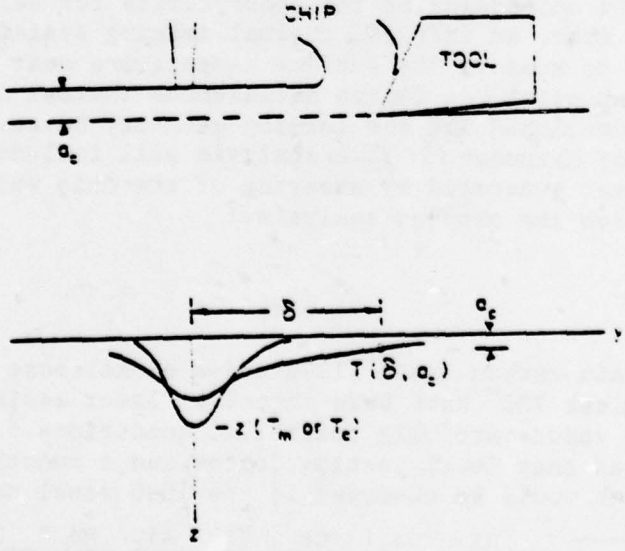

Fig. 4. Temperature distribution in workpiece due to laser beam heating.

Cline and Anthony give temperature distributions in terms of a dimensionless temperature $f(x,y,z,V)$ and dimensionless distances x/R_b or z/R_b, where

$$T(x,y,z) = \alpha P(C_p \kappa R_b)^{-1} f(x,y,z,V) \quad (1)$$

where

T = temperature at (x,y,z) in ^{o}C
α = absorptivity
P = incident power (W)
c_p = specific heat per unit volume ($Jcm^{-3}\ ^{o}C^{-1}$)
κ = thermal diffusivity (cm^2s^{-1})
R_b = focussed beam radius (cm)

Each temperature distribution is characterized by a dimensionless number R_bV/κ where V is the cutting velocity in cms^{-1}. To calculate the temperature of the workpiece at the cutting tool edge $T(\delta,a_c)$, we employ the Green's function solution for a point source moving at a constant velocity

$$T = \frac{\alpha P}{C_p \kappa 2\pi r} \exp\left(-\frac{V(r+x)}{2\kappa}\right) \quad (2)$$

The undeformed chip thickness a_c equals the feed. In our calculations, we assume $\alpha = 0.10$. Currently, measurements are being carried out in our laboratory to determine the temperature dependence of the absorptivity for selected materials. Also, an infrared thermal imaging system is being installed to measure the surface temperature near the beam impingement point. A finite differences thermal analysis is being developed for the turning geometry based on the approach of Mazumder.(5) This analysis will include the effect of heat generated by shearing of the chip which is omitted from the present analysis.

Results

A plain carbon steel (1090) and a nickel base superalloy, Udimet 700* have been shaped by laser assisted machining under carefully controlled conditions.[2] It was anticipated that lower cutting forces and a smoother surface finish would be observed in the 1090 steel due to con-

* U-700 (wt pct)

Ni	Co	Cr	Ti	Al	Mo	C	B
Bal	18.5	15.0	3.5	4.3	5.3	0.08	0.030

version of material in front of the tool to supercooled austenite. In the case of the Udimet 700, it was anticipated that lower cutting forces and a smoother surface finish would be observed due to formation of a rapidly solidified microstructure in front of the cutting tool and due to heating of the workpiece material to a temperature such that yield stress was decreased.

The 1090 steel was machined at a cutting velocity of 17.1 cm s^{-1} (33.4 ft min^{-1}). The feed (f) was 0.0125 cm and the back engagement (a_p) was 0.0250 cm. The distance (δ) from the laser beam impingement point to the cutting tool edge was 0.4 cm. The incident power measured at the workpiece was 460 W. The laser was operated at a wavelength of 10.6 μm in the TEM_{oo} (Gaussian) mode. The beam was focussed to a radius of 0.0065 cm giving an incident power density of 3.5×10^6 W cm^{-2}.

To calculate the temperature distribution for the 1090 steel during laser assisted machining, we set c_p = 3.56 J cm^{-3} s^{-1} and κ = 0.143 cm^2 s^{-1}(6). This gives $\alpha P(c_p \kappa R_b)^{-1}$ = 13,900°C. For the melting isotherm T = 1539°C and f = 0.11. The parameter R_b V/κ = 0.8. From Fig. 6 of Ref. (4) $z(T_m)/R_b$ = 0.3 or $z(T_m)$ = 19.5 μm. For the eutectoid isotherm, T = 723°C and f = 0.052. This gives $z(T_c)/R_b$ = 1.2 or $z(T_c)$ = 78μm. The temperature of the workpiece at the cutting tool edge $T(\delta, a_c)$ is given by Eqn. 2 to be T(0.4, 0.0125) = 62°C.

The results of this thermal analysis are in agreement with our previous observations (2). We found that, in contrast to our hopes, tool forces increased rather than decreased when we cut the 1090 steel with the laser beam. It appears that a fraction of the undeformed chip volume was austenitized by laser beam heating but this volume cooled below the M_s temperature (238°C) before encountering the cutting edge of the tool. It should be noted, however, that the depth to which the workpiece was austenitized may have exceeded 78μm, because the absorptivity probably exceeded 0.1 due to surface melting.

The Udimet 700 was machined at a cutting velocity of 28.2 cm s^{-1} (54.9 ft min^{-1}). The feed was 0.0125 cm and the back engagement was 0.0250 cm. The laser irradiation conditions were the same as for the 1090 steel.

To calculate the temperature distribution for Udimet 700 during laser assisted machining we set c_p = 3.43 J cm^{-3} $°C^{-1}$ and κ = 0.06 cm^2 s^{-1}(6). This gives $\alpha P(c_p \kappa R_b)^{-1}$ = 33,890°C. For the melting isotherm, T = 1300°C and f = 0.038. The parameter R_b V/κ = 3.06. From Fig. 6 of Ref. (4), $s(T_m)/R_b$ = 0.7 or $s(T_m)$ = 45.5 μm. The temperature of the workpiece at the cutting tool edge is given by Eqn. 2 to be 109°C.

The results of this thermal analysis are also in agreement with our previous observations (2). We found that surface finish and tool life were improved in laser assisted machining of Udimet 700 but that tool forces were unchanged. It appears that a fraction of the undeformed chip volume should have been melted by the laser beam. Since this volume would have been rapidly quenched, its microstructure could have been altered sufficiently to account for the observed improvements. It does not appear, however, that workpiece material arriving at the cutting edge could have retained enough heat to decrease the cutting force. It is estimated that workpiece temperatures of about 1000°C at the cutting edge would have been necessary to lower the yield stress sufficiently to decrease the cutting force. As discussed, in the case of the 1090 steel, the depth to which the Udimet 700 melted may have exceeded 45.5 μm due to increased absorptivity upon melting.

Effects at Higher Power

We have recently purchased, with funds from a grant by the National Science Foundation, a 1400 W CW CO_2 laser. It is interesting to predict the results of laser assisted machining at this level of incident power.

In the case of 1090 steel, if we consider the same cutting velocity (17.1 cm s^{-1}) and set αP = 140 W, we calculate $\alpha P\ (c_p \kappa R_b)^{-1}$ = 42,300°C and R_b V/κ = 0.8. For the melting isotherm, f = 0.036, so from Fig. 6, Ref. (4), $s(T_m)/R_b$ = 1.7 or $s(T_m)$ = 110μm. For the eutectoid isotherm, f = 0.017, so $s(T_c)/R_b$ = 2.5 or $s(T_c)$ = 162μm. The temperature of the workpiece at the cutting tool edge is given by Eqn. 2 to be T(0.4, 0.0125) = 135°C, which is less than the M_s temperature. However, taking into consideration that: (i) the actual absorptivity may exceed 0.10 due to surface melting; (ii) in the turning configuration, cooling at the edge of the workpiece will be less efficient than in the

case for which the calculation was made, and (iii) the high shear strain rates associated with chip formation also heat the workpiece material, we conclude that it is likely that the actual temperature of the workpiece material of the tool edge will exceed the M_s temperature. If we ignore these considerations, however, we calculate with Eqn. 2 that it is possible to obtain the M_s temperature (238°C) either by increasing the absorbed power, αP, to 333 W or by decreasing the distance (δ) from the laser beam to the cutting edge of the tool to 0.17 cm.

In the case of Udimet 700, we will set $\alpha P = 140W$ and consider a somewhat lower velocity 15.2 cm s^{-1} (30 ft min^{-1}) than that previously considered 28.2 cm s^{-1} (54.9 ft min^{-1}). This lower velocity is comparable to that employed with carbide tools in current machining practice. We calculate $\alpha P(c_p \kappa R_b)^{-1} = 103{,}000°C$ and $R_b V/\kappa = 1.65$. For the melting isotherm, $f = 0.013$ so from Fig. 6, Ref. (4) $s(T_m)/R_b = 2$ or $s(T_m) = 0.0130$ cm. The temperature of the workpiece at the cutting tool edge $T(0.4, 0.0125) = 286°C$. Thus it appears possible in Udimet 700 to melt and rapidly solidify the workpiece material before it encounters the cutting tool edge. In materials such as the superalloys containing hard carbide particles this should result in improved tool life. Further, solutionizing the gamma prime precipitate particles in Udimet 700 may increase tool life and decrease surface roughness by decreasing the tendency to form a built up edge.

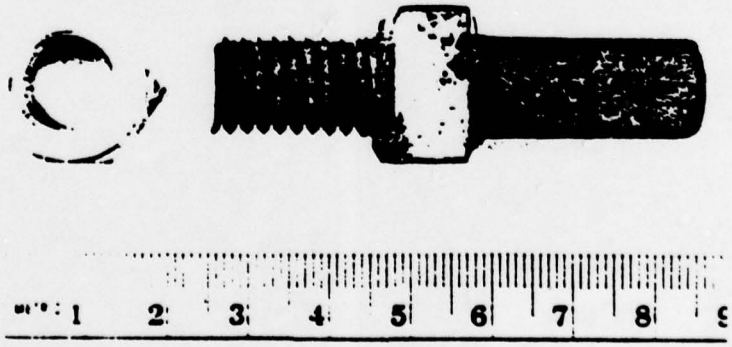

Fig. 5. Laser turned and threaded SiAlON.

LASER MACHINING

Figure 5 shows a laser machined piece of SiAlON, which originally had a 2cm x 2cm square cross section. One end has been turned to a circular cross-section 1.25 cm in diameter. A $\frac{1}{4}$in x 13 screw thread has been machined in the other end. The method for laser machining screw threads is described in Ref. (3).

Laser machining is based on the overlapping of grooves cut by the laser beam as it scans the surface of the work-piece. Figure 6 shows two such grooves formed in SiC at different cutting velocities. Groove 2 was formed at a velocity of 0.155 m s^{-1} and groove 18 was formed at 0.055 m s^{-1}. The shape of the grooves approximates the spatial distribution of power of the beam, which was Gaussian. In Si_3N_4 and SiAlON to grooves are believed to form by the reaction

$$Si_3N_4 + 7/2\ O_2 \rightarrow 3SiO(g) + 4\ NO(g)$$

while in SiC, by the reaction

$$SiC + O_2 \rightarrow SiO(g) + CO(g)$$

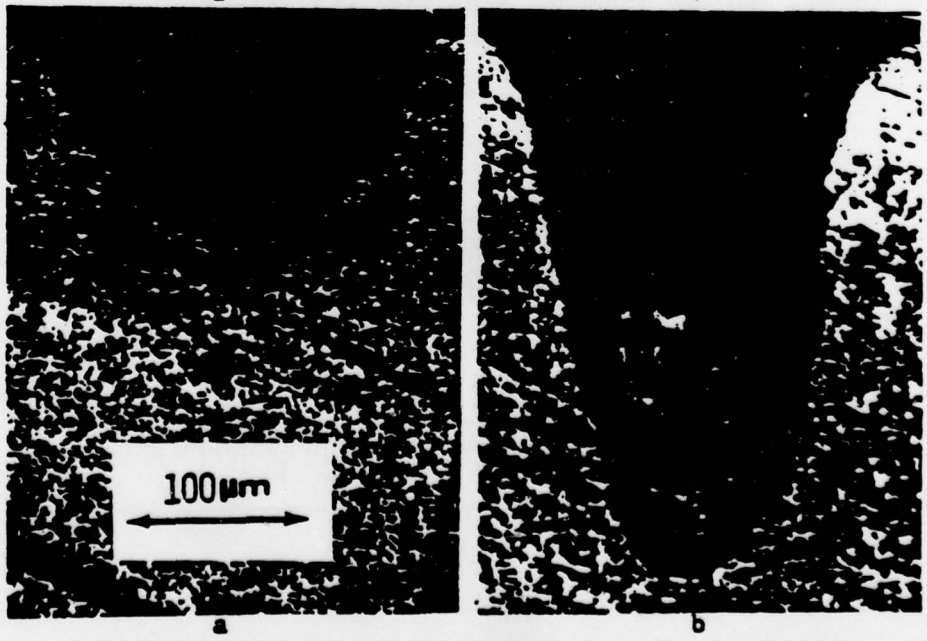

Fig. 6. Cross section of laser machined grooves in SiC (a) groove number 2, (b) groove number 18.

Table 1. Parameters Describing Laser Machined Grooves[3]

Groove	$V(ms^{-1})$	D(μm)	a(μm)	$A_{calc}=Da\sqrt{\pi}\ m^2$	$A_{meas.}\ m^2$
1	0.165	96	83	14.1×10^{-9}	13.8×10^{-9}
5	0.140	121	81	17.4×10^{-9}	17.1×10^{-9}
8	0.120	139	83	20.4×10^{-9}	19.8×10^{-9}

Specific Machining Energy

The authors have shown that the depth of grooves formed by a CW CO_2 laser in SiC varies linearly with the dwell time θ, which is defined as the focussed beam diameter divided by the beam velocity, Fig. 7. For dwell times less than 1.4×10^{-3}s, the slope was found to increase so than an extrapolation of the data to zero dwell time predicts a groove depth, D = 0.

Table 1 gives parameters corresponding to three of the grooves formed at dwell times less than 1.4×10^{-3} s.

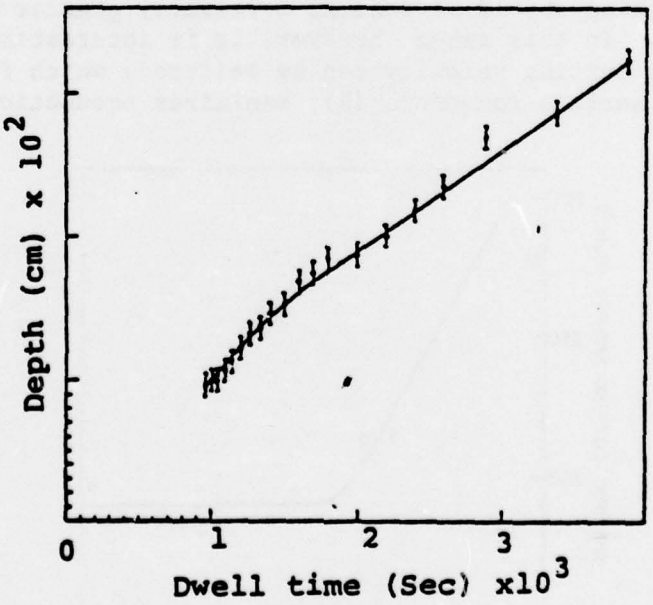

Fig. 7. Depth of laser machined grooves in SiC versus dwell time. The incident power of the laser beam was 450 W and it was focussed to a $1/e^2$ diameter of 160μm.

The parameter a is the half width of the groove at 1/e of its depth. It is independent of velocity and approximately equals one half the beam diameter. The parameter A_{calc} is the cross-sectional area of the groove calculated from the measured values of D and a assuming that the shape of the grooves is Gaussian. The parameter A_{meas} was obtained by graphical integration of the area obtained from a tracing of the grooves. The close agreement of A_{calc} and A_{meas} verifies approximating the shape of the grooves by a Gaussian.

The material removal rate $\dot{z} = A V$ and the specific cutting energy $\rho = P/\dot{z}$, where P is the incident beam power. Figure 8 shows a plot of specific machining energy versus cutting velocity. At high velocities, corresponding to dwell times less than 1.4×10^{-3} s, the specific machining energy becomes a constant equal to 190 GJ m^{-3}.

Optimum Machining Parameters

The dependence of the specific machining energy on cutting velocity suggests that for most efficient material removal, cutting should be done at a velocity greater than 0.08 ms^{-1}. In this range, however, it is interesting that an optimum cutting velocity can be selected, which for a specified surface roughness (R), minimizes production time and cost.

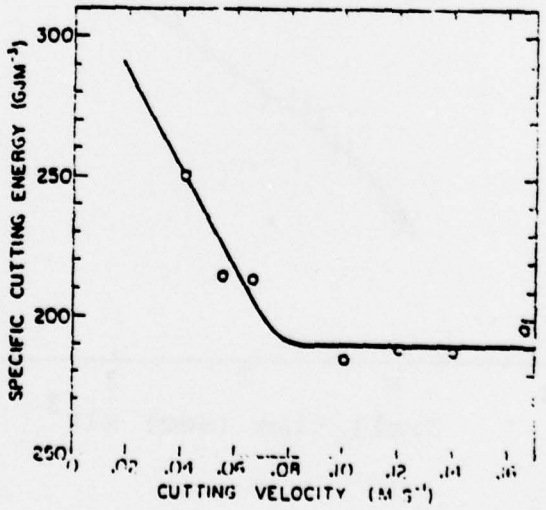

Fig. 8. Specific machining energy versus cutting velocity.

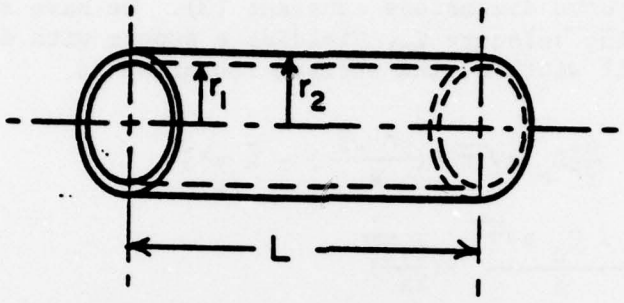

Fig. 9. Workpiece for calculating optimum machining parameters.

Consider, for example, the task of turning the workpiece shown in Fig. 9 from an initial radius r_2 to a final radius r_1 over a distance L. The total time for this task can be represented by the equation

$$t_{total} = t_c + t_{npr} \tag{3}$$

where t_c is the time spent cutting and t_{npr} is the time spent returning the beam to its starting position after the cut has been made. The cutting time can be written as the volume to be removed $\pi L(r_2^2 - r_1^2)$ divided by the effective material removal rate. For overlapping grooves the effective material removal rate $\dot{z}' = Dvf$. The nonproductive time is $n\Delta t_r$, where n is the number of cuts required to shape the workpiece and Δt_r is the carriage return time. The number of cuts is $(r_2 - r_1)/D$ and the return time is $c_1 L$, where c_1 is a constant. Thus Eqn. 3 can be rewritten

$$t_{total} = \frac{\pi L(r_2^2 - r_1^2)}{Dvf} + \frac{c_1 L(r_2 - r_1)}{D} \tag{4}$$

for $V < V^*$, $D = c_2 V^{-1}$, and thus

$$t_{total} = \frac{\pi L(r_2^2 - r_1^2)}{c_2 f} + \frac{c_1 L(r_2 - r_1)v}{c_2} \tag{5}$$

For a specified surface roughness (R), the feed is a function of velocity, because velocity determines the shape of the groove. We have previously shown how to calculate the dependence of surface roughness on feed, holding velocity and thus groove dimensions constant (3). We have shown that for a cutting velocity V_o, yielding a groove with depth D_o and 1/e half width a, the surface roughness is

$$R_o = \frac{4}{f}\left[D_o\, a\sqrt{\pi}\, F\left(\frac{y^* \sqrt{2}}{a}\right) - \bar{D}\, y^*\right] \tag{6}$$

where

$$\bar{D} = \frac{2\, D_o\, a\sqrt{\pi}}{f}\, F\left(\frac{f\sqrt{2}}{2a}\right) \tag{7}$$

and

$$y^* = \frac{a}{\sqrt{2}}\, f^{-1}\left(\frac{\bar{D}}{D_o \sqrt{2\pi}}\right) \tag{8}$$

In these equations

$$f(w) = \frac{1}{\sqrt{2\pi}}\, \exp\left(-\frac{w^2}{2}\right) \tag{9}$$

$$F(w) = \int_o^w f(w)\,dw \tag{10}$$

If we choose $V_o = 0.165\ m\ s^{-1}$ (Groove 1, Table 1), then a plot of R_o and a versus f can be obtained as shown in Fig. 10. The dependence of R_o on f can be expressed by the function $R_o = c_3 f^n$.

Examination of Eqns. 6-8 reveals that as long as a remains constant and $D = c_2 V^{-1}$, the roughness R at a velocity V is related to the roughness R_o at a velocity V_o by the equation

$$R = \frac{R_o V_o}{V} \tag{11}$$

Thus we may write

$$f = \left(\frac{RV}{c_3 V_o}\right)^{\frac{1}{n}} \tag{12}$$

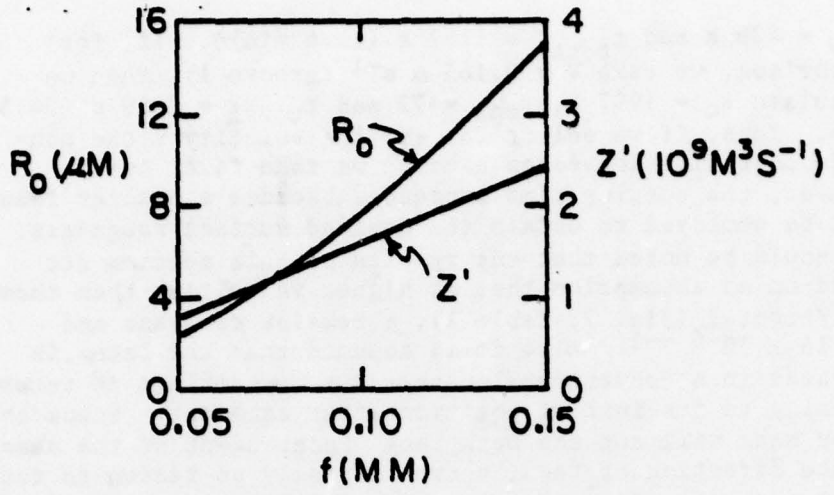

Fig. 10. Roughness and effective material removal rate versus feed.

Substituting for f in Eqn. 5, we obtain

$$t_{total} = \frac{\sqrt{\pi}\, L(r_2^2 - r_1^2)}{c_2} \left(\frac{R}{c_3 V_o}\right)^{-\frac{1}{n}} V^{-\frac{1}{n}} + \frac{c_1 L(r_2 - r_1)}{c_2} V \tag{13}$$

To obtain the cutting velocity for minimum production time to produce a specified surface roughness, we equate the first derivative of t_{total} with respect to V to zero and solve for V. This gives

$$\left[V_{min} = \frac{\sqrt{\pi}(r_1 + r_2)}{n\, c_1} \left(\frac{R}{c_3 V_o}\right)^{\frac{1}{n}}\right]^{\frac{n}{n+1}} \tag{14}$$

The constant c_2 can be determined from Fig. 7 to be $16 \times 10^{-6} m^2 s^{-1}$. The constants c_3 and n can be determined from Fig. 10 to be $64.7 m^{0.577}$ and 1.73, respectively. Let us assume $L = 12.5 \times 10^{-3} m$ $r_2 = 12.5 \times 10^{-3} m$ and $r_1 = 9.0 \times 10^{-3} m$ and that the desired surface roughness is 6.7 μm (N9). The constant c_1 can be calculated to be 160 $s\ m^{-1}$ if the time spent returning the laser beam to its initial position is assumed to be 2s. Substituting these values into Eqn. 14, we calculate $V_{min} = 0.98\ m\ s^{-1}$, $t_c = 738$ s,

t_{npr} = 429 s and t_{total} = 1167 s (19.4 min)*. If, for comparison, we take V = 0.165 m s^{-1} (groove 1), then we calculate t_c = 1997 s, t_{npr} = 72 and t_{total} = 2069 s (34.5 min). Thus, if we select too small a velocity V the non-productive time decreases because we take fewer cuts; however, the cutting time increases because a smaller feed must be employed to obtain the desired surface roughness. It should be noted that the results of this section are based on an assumption that at higher velocities than those investigated (Fig. 7, Table 1), a remains constant and $D = 16 \times 10^{-6} V^{-1}$. Also it is assumed that the lathe is operated in a conventional manner, i.e the carriage is returned manually to its initial position after each cut. Since the laser beam will cut the workpiece independent of the sense of the direction of feed, there is really no reason to turn the laser beam off and return the carriage to its initial condition. If the laser is allowed to cut for both positive and negative feeds, the velocity for minimum production time will be the largest that will still vaporize the workpiece.

References

(1) W. W. Duley., "CO_2 Lasers, Effects and Applications" Acad. Press, New York, 1976.

(2) M. Bass, S. M. Copley and D. Beck, "Laser Assisted Machining", Proceedings of the 4th European Electrooptic Conference, Utrecht, Netherlands, 1978.

(3) S. M. Copley, M. Bass and R. G. Wallace, "Shaping Silicon Compound Ceramics with A Continuous Wave Carbon Dioxide Laser", Proceedings of 2nd International Symposium on Ceramic Machining and Finishing, Gaithersburg, Md., 1978.

(4) H. E. Cline and T. R. Anthony, "Heat Treating and Melting Materials with A Scanning Laser or Electron Beam", J. Appl. Phys. Vol. 48, p. 3895-900, 1977.

(5) J. Mazumder, Ph.D. Thesis, London University, 1977.

(6) Handbook of Materials Science, C. T. Lynch, Ed., CRC Press, Cleveland, Ohio, 1975.

---

* This value is greater than that reported in Table 3, Ref. (3) which was based on a groove with D = 125 μm and a = 100 μm.